Damage Mechanisms of Porous Materials due to In-Pore Salt Crystallization

Mara Schiro, Encarnacion Ruiz-Agudo, and Carlos Rodriguez-Navarro*

Department of Mineralogy and Petrology, University of Granada, Fuentenueva s/n, 18002 Granada, Spain

(Received 24 July 2012; revised manuscript received 12 November 2012; published 26 December 2012)

Pressure exerted by crystallization of salts within porous materials contributes to damage in historic and modern construction. By unequivocally identifying the precipitating phase(s) while simultaneously determining solution supersaturation and associated crystallization pressure in subsurface pores, we show that the formation of a thermodynamically metastable salt phase (heptahydrate; $Na_2SO_4 \cdot 7H_2O$) and the resulting transition to a less soluble stable phase (mirabilite; $Na_2SO_4 \cdot 10H_2O$) is largely responsible for the high supersaturation and crystallization pressure developed during evaporative crystallization of sodium sulfate, the most damaging salt known. These results help to explain why salts with various (stable and metastable) hydrated phases are the most damaging. We also show that damage associated with metastable-stable phase transitions can be suppressed by the use of crystallization promoters. These results open new ways for the prevention of salt damage to building materials.

DOI: 10.1103/PhysRevLett.109.265503 PACS numbers: 61.05.cp, 64.70.dg, 64.70.fm, 81.10.Dn

Crystallization in confined spaces, such as pores, is relevant to nearly every field of science, from industrial concerns related to pipe clogging in heating, cooling, and oil recovery systems [1,2], to pore blockage in CO_2 sequestration [3], cement setting [4], crystal growth in gels [5], biomineralization [6], and conservation of construction affected by frost [7] and salt damage [8]. A fundamental understanding of crystal nucleation, phase transition, and growth in a confined geometry is critical to controlling these processes and avoiding undesired effects such as salt weathering [7,8], which is considered a leading cause of damage to sculptural and built heritage [4,7–15].

As first suggested by Thomson in 1862 [16], the main mechanism by which salts cause damage is by generating crystallization pressure [13]. The crystallization pressure (Δp) exerted by a crystal in a pore can be calculated by [7,13,17,18]

$$\Delta p = \frac{RT}{V_m} \ln\frac{\mathrm{IAP}}{k_s} - \gamma_{\mathrm{cl}}\kappa_{\mathrm{cl}} + \frac{\Delta V}{V_m}\gamma_{\mathrm{lv}}\kappa_{\mathrm{lv}} \qquad (1)$$

where IAP is the ion activity product, k_s is the solubility product (IAP/k_s is the supersaturation, β), $\Delta V = \Sigma V_L - V_m$, $V_L = \Sigma V_i$ is the sum of ion molar volumes, V_m is the crystal molar volume, κ_{cl} and κ_{lv} are the curvature of the crystal-solution and liquid-vapor interfaces, respectively, and γ_{cl} and γ_{lv} are the crystal-solution and vapor-solution surface energies. The first term shows that Δp depends on supersaturation, which acts as a driving force for salt damage [4]. The second and third terms are of insignificant magnitude in pores >100 nm [13,19].

The three kinetic pathways by which high β and Δp are commonly produced are (a) rapid drying [7,10,14]; (b) rapid cooling of salts with T-dependent solubilities [12,20]; and (c) formation of a saturated solution with respect to one phase (i.e., dissolution of thenardite, Na_2SO_4) but supersaturated with respect to another (i.e., mirabilite) [19,21]. While some progress has been made in understanding the second and third pathways [12,19], little is known about the common and highly deleterious case in which Δp is generated during evaporation, especially in salt systems with multiple hydrated phases (Fig. 1). These hydrated salt systems (e.g., sodium sulfate, sodium carbonate, and magnesium sulfate) are the most damaging [9,22], despite the fact that their high solubilities and correspondingly very low γ_{cl} values [13], should mean that these systems will crystallize before a high supersaturation is sustained.

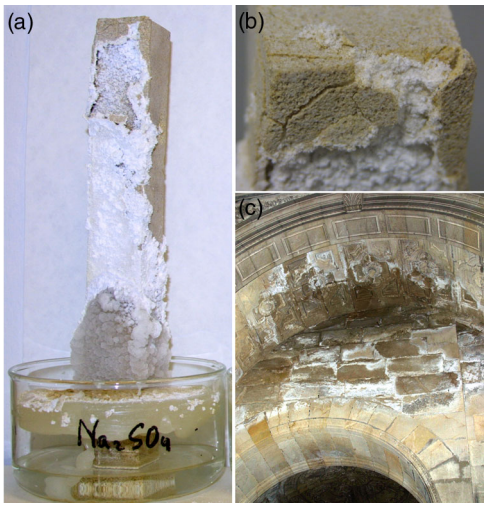

FIG. 1 (color online). Salt damage of porous building materials. (a) Limestone block showing extensive damage due to sodium sulfate crystallization. Capillary rise and continuous evaporation over 1 week led to massive efflorescence in the bottom portion of the block and subflorescence (in-pore salt crystallization) and associated damage near the top of the block. (b) Detail of damage on the top part of the limestone block. (c) Example of salt damage (sodium sulfate) in the interior of the Granada Cathedral complex (Sagrario Chapel).

A critical and challenging experimental task is the determination of which a salt phase crystallizes in a pore and at what supersaturation. Other researchers have used differential scanning calorimetry (DSC) [20] and nuclear magnetic resonance in combination with synchrotron energy-dispersive diffraction with hard x rays [12] to quantify solution supersaturation and to identify the crystallizing phase in porous media during cooling-induced sodium sulfate crystallization. However, cooling-induced crystallization is unrepresentative of most natural environments where crystallization follows evaporation of a saline solution [10]. To study this complex situation, we used a combination of instrumental techniques (see Materials and Methods in Supplemental Material [23]): (a) two-dimensional x-ray diffraction (2D-XRD; using highly penetrative Mo $k\alpha$ radiation) to identify the in-pore sequence of crystallizing phases, (b) thermal gravimetry (TG) combined with DSC to calculate the supersaturation with respect to each crystallizing phase as well as Δp according to the first term in Eq. (1) following a Pitzer parametrization (see Ref. [18] and Supplemental Material [23]), and (c), environmental scanning electron microscopy (ESEM) to study the *in situ* evaporative crystallization of sodium sulfate at high magnification [14]. We choose to study sodium sulfate because it forms different hydrated and anhydrous phases, it is the most deleterious salt known, and it is ubiquitous both in nature and in old and modern construction [10].

TG analysis of a 1 M Na_2SO_4 solution evaporating from a model porous substrate (glass frits [23]) allows for the determination of the precise evaporation rate and the calculation of the concentration of the solution at every point during evaporation. The heat flow was measured using DSC throughout evaporation and crystallization within the porous substrate. With the concentration of the solution known for every point in time (from TG) and the precise timing of crystallization identified (from DSC), we determined the solution concentration at the onset of crystallization (Fig. 2; see also Supplemental Material [23]). The DSC trace shows a broad exothermal event with two relative maxima corresponding to different crystallization events, followed by an endothermal event, both overprinted on the general endothermal evaporation curve [Fig. 2(a)]. 2D-XRD [Figs. 2(b) and 2(c)] shows the sequential formation of heptahydrate, mirabilite, and thenardite. We observed a reduction in the intensity of heptahydrate Bragg peaks (and their final disappearance) coupled with an increase in the intensity of mirabilite Bragg peaks as evaporation and crystallization progressed [Figs. 2(b) and 2(c)]. This crystallization sequence follows the Ostwald's rule of stages, which states that metastable phases precede the formation of stable ones [24]. Our results point to a heptahydrate to mirabilite phase transition taking place via solvent-mediated dissolution-precipitation [24,25]. Because heptahydrate cannot spontaneously dissolve back into its own saturated solution [20], its dissolution must occur concurrently with mirabilite precipitation. The lower crystal-liquid interfacial energy of metastable heptahydrate (0.027 $N\,m^{-1}$) [20] compared with mirabilite (0.043–0.06 $N\,m^{-1}$) [11,13] favors the initial in-pore crystallization of heptahydrate at a lower β. This is in agreement with calculations of the nucleation density I^B of both hydrated phases (Supplemental Material, Fig. 1 [23]). Formation and transformation of metastable phases in salt systems with different hydrates appears to be a general phenomenon, as recently demonstrated for the $CaSO_4$-H_2O system [2].

2D-XRD results show that thenardite Bragg peaks appear and grow in intensity as mirabilite peaks disappears [Figs. 2(b) and 2(c)]. The presence of a well-defined endotherm in the DSC trace [Fig. 2(a)], is consistent with the formation of thenardite following dehydration of mirabilite via a solid-state reaction.

In a porous substrate, evaporation initially occurs at the substrate surface controlled by constant drying rate kinetics and is followed by a period of diffusion-controlled evaporation kinetics [see Refs. [26,27] and Supplemental Material [23]). In all of our experiments, the Péclet number, Pe during the first drying stage is 0.9 to 2.1, and 0.1 to 0.5 during the onset of crystallization, which systematically took place during the second stage of drying (see Supplemental Material [23]). A $\mathrm{Pe} < 1$ means that solute transport during the crystallization stage is diffusion controlled [28].

The combined data from TG, DSC, and 2D-XRD show that when the concentration of the solution reached 3.04 (22.54 °C) to 3.44 m (molal) (22.58 °C), heptahydrate precipitated from solution ($\beta \sim 1$). When plotted in the Na_2SO_4-H_2O phase diagram (Fig. 3), these values fall within the range of published solubility data for heptahydrate. In no case did crystallization of heptahydrate occur at a concentration corresponding to the supersolubility curve. Nuclear magnetic resonance has also shown nucleation of heptahydrate within porous supports once the solubility curve is reached [11]. This is most probably due to the fact that the porous substrate offers numerous sites for heterogeneous nucleation. Heptahydrate is metastable and as soon as mirabilite starts to nucleate, undersaturation with respect to heptahydrate will lead to its dissolution. The resulting solution is supersaturated with respect to mirabilite ($\beta = 2.45$). For the observed critical β of mirabilite, a Δp of 10 MPa is generated. In practice, the calculated Δp is not exactly equal to the stress created during a crystallization event, since pressure is not effectively transmitted through a porous body [20]. Applying poroelasticity theory, the effective stress, P can be calculated by $P = b\phi_e \Delta p$, where b is the Biot coefficient and ϕ_e is the volume fraction of pores filled with salt crystals [19] (see details in SM [23]). In our porous material, the effective stress would be 2.4 MPa ($\phi_e = 0.27$). This is sufficient to cause damage to building materials such as the limestone in Fig. 1, which has a (dry) tensile strength, σ_T of 1.8 ± 0.5 MPa and 28% porosity. The porous glass has a higher σ_T of 6.3 ± 1.2 MPa, which may prevent damage. Note, however, that σ_T of moisture saturated porous materials tend to be ~40% lower than for the dry material, as observed here for the limestone (1.1 ± 0.2 MPa) and the porous glass (4.2 ± 0.6 MPa). While the calculated effective

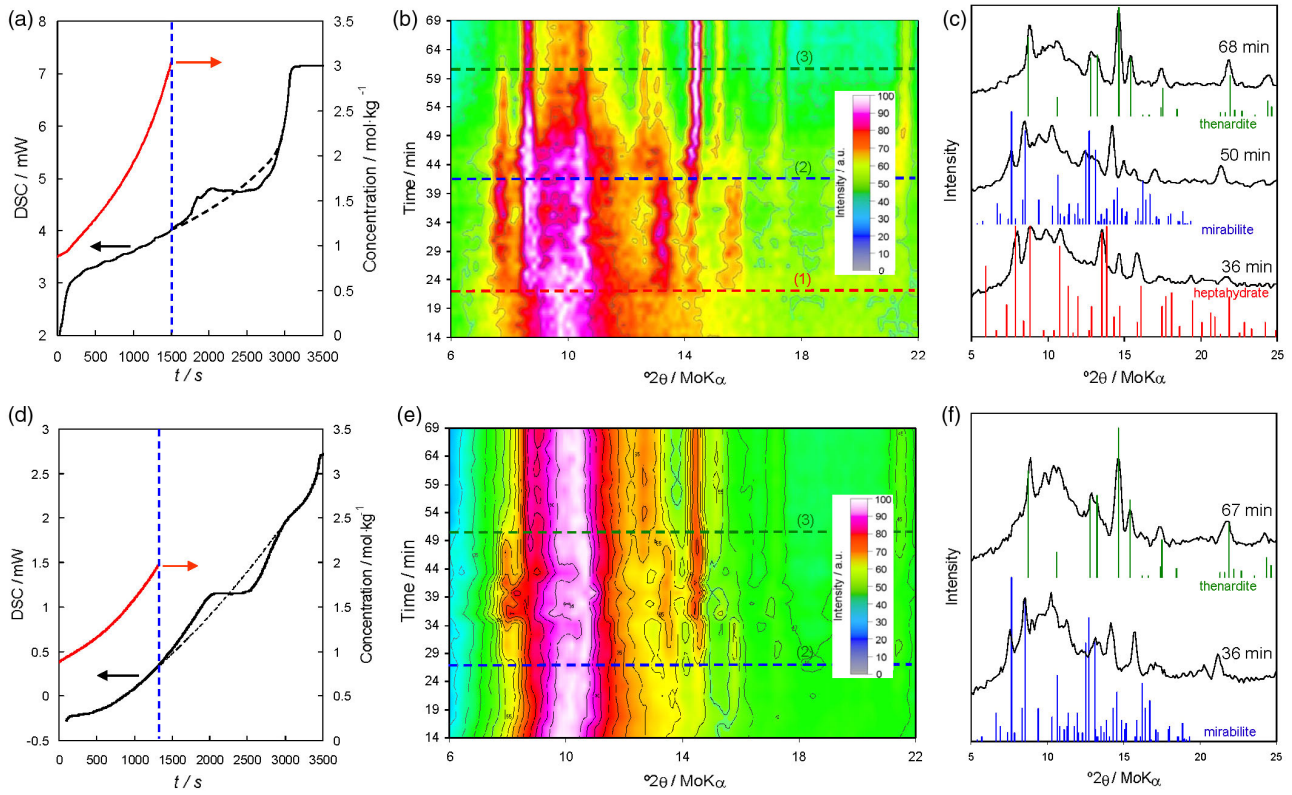

FIG. 2 (color online). Crystallization of sodium sulfate within porous media. (a) Evolution of the solution concentration (TG) and heat evolved (DSC) during evaporative crystallization. The onset of crystallization is indicated by the vertical dashed (blue) line. Dashed (black) line in DSC trace shows modeled heat evolution associated with solution drying assuming no sodium sulfate crystallization or dehydration. (b) Intensity map of sequential 2D-XRD patterns showing the initial crystallization of heptahydrate [marked by the horizontal dashed (1) red line], which starts to disappear [marked by the dashed (2) blue line] as shown by the reduction in intensity of its main Bragg peaks concurrently with the appearance of the main mirabilite Bragg peaks; finally, mirabilite starts to disappear (dehydrates) as thenardite Bragg peaks become most intense [marked by the dashed (3) green line]. (c) XRD patterns corresponding to the sequential formation of heptahydrate, mirabilite, and thenardite. The XRD line patterns of each phase are shown as a reference (red: heptahydrate [31]; blue: mirabilite, JCPDS card 11-0647; green: thenardite, JCPDS card 37-1465). (d) Same as (a) but following evaporative crystallization of sodium sulfate in the presence of 0.01 M borax. (e) Same as (b) but showing the initial precipitation of mirabilite in the presence of borax, followed by the formation of thenardite after mirabilite dehydration. (f) XRD patterns corresponding to mirabilite formation in the presence of borax and its dehydration to form thenardite.

stress may not be high enough to cause massive failure of a porous material, it will likely result in the formation of microcracks and fractures. Multiple crystallization events taking place over longer periods of time can result in cumulative damage [22]. Note that periodic crystallization events typically occur following continuous supply of saline solution during evaporative crystallization in porous materials [22] and lead to substantial damage, as shown in Fig. 1.

TG, DSC, and 2D-XRD experiments were repeated with the addition of 0.01 M borax or 0.01 M DTPMP (diethylenetriamine-penta-methylene phosphonic acid) to the 1 M Na_2SO_4 solution. Borax promotes the crystallization of mirabilite at or near saturation [29], while inhibiting heptahydrate formation. DTPMP is commonly used as a scale inhibitor [1]. In solution, DTPMP molecules inhibit sodium sulfate crystallization, while their adsorption on a substrate favors the heterogeneous nucleation of salts [1]. This dual role (inhibitor and promoter) is shown by many organic molecules in biomimetic crystallization and biomineralization [6]. These DSC results show only one exotherm followed by one endotherm overprinted on the general endothermal curve, corresponding to the evaporation of the solution in the presence of DTPMP or borax [Fig. 2(d)]. Regardless of the type of additive used (borax or DTPMP) 2D-XRD [Figs. 2(e) and 2(f)] shows that these events correspond chronologically to the crystallization of mirabilite and its dehydration to thenardite. From TG, the concentration of the solution at the onset of mirabilite crystallization, which occurred during the second stage of drying ($Pe < 1$), was calculated to be 1.77 (23.7 °C) to 1.97 m (24 °C), with $\beta = 1.00$–1.12 (Fig. 3). Under these concentrations, the solution is undersaturated with respect to heptahydrate. Δp of mirabilite for the highest β value is 1.3 MPa, and P is 0.18 MPa ($\phi_e = 0.16$): not enough to create damage to most building materials [4,21]. These results demonstrate that additives (crystallization promoters) have the potential to inhibit or at least significantly

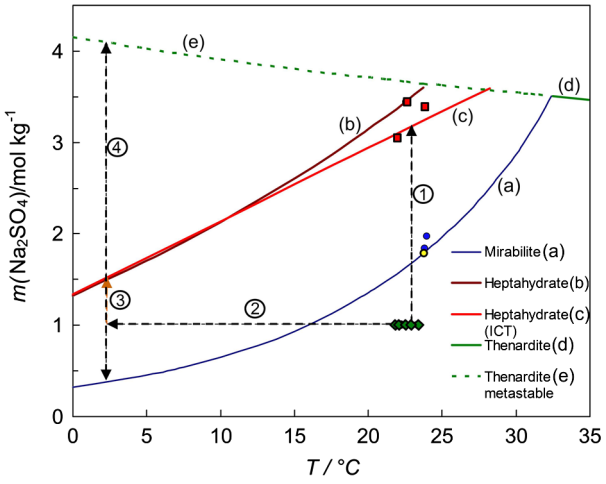

FIG. 3 (color online). The T-dependent solubility diagram of the system Na_2SO_4-H_2O. This diagram shows the solubility curves of mirabilite [curve (a)], heptahydrate (values from Refs. [18] curve (b); and ICT [32], curve (c)), and thenardite [phase V; curve (d)], as well as the metastability curve of the latter from Ref. [18] [curve (e)]. Concentration values at the onset of crystallization in glass frits (TG-DSC results) are plotted [green solid diamond: initial 1 M Na_2SO_4; red solid square: onset of heptahydrate crystallization; blue solid circles and yellow solid circle (empty circle in printed version): onset of mirabilite crystallization in the presence of borax and DTPMP, respectively]. The dashed black arrow (1) shows the solution concentration evolution during evaporative crystallization. Dashed arrows (2) and (3) (brown) show the T and concentration evolution during ESEM crystallization cycles where only hydrated phases were formed. Dashed arrow (4) (black) shows the concentration path during ESEM crystallization cycles involving anhydrous and hydrated phases.

reduce the physical damage that results from evaporative salt crystallization in porous materials.

When thenardite, particularly fine-grained crystals, is exposed to water, it rapidly dissolves, producing a solution saturated with respect to thenardite, and thus highly supersaturated with respect to mirabilite [21]. Subsequent mirabilite crystallization results in significant damage [14]. *In situ* XRD [30] and synchrotron hard x-rays diffraction [19] have shown that thenardite dissolution within a porous material (glass frits and limestone) at room T is followed by mirabilite crystallization. The reason why no heptahydrate precursor forms is not known, although it could be argued that undissolved thenardite crystals act as seeds for direct mirabilite crystallization due to the similarities in their crystal structures.

In an attempt to isolate the damage caused by the thenardite-mirabilite transition, from that of the initial drying-induced crystallization sequence heptahydrate-mirabilite, ESEM images were captured during crystallization and dissolution cycles at 2 °C, where drying was stopped upon crystallization of the sodium sulfate hydrated phase, before dehydration to thenardite [Fig. 4(a)]. pH_2O was then increased at constant T to dissolve all hydrated crystals and a second crystallization event of hydrated sodium sulfate was promoted (Fig. 3). At 2 °C dissolution of heptahydrate results in a solution supersaturated with respect to mirabilite ($\beta = 6.79$), which crystallizes yielding a value of $\Delta p = 19.9$ MPa, and $P = 1.94$ MPa ($\phi_e = 0.11$). Such effective stress is smaller than the (wet) tensile strength of the porous glass and should not lead to damage. However, some damage was observed [Fig. 4(b)]. This is most probably due to the fact that fast evaporation in the ESEM chamber led to concentration gradients (i.e., Pe > 1) and a higher salt pore filling. The fact that efflorescence is observed on the substrate [Figs. 4(a) and 4(b)] supports that Pe > 1. Assuming a limiting situation where total pore filling by salt occurs due to advective transport (i.e., $\phi_e = 0.28$), a maximal P value of 4.95 MPa will be achieved. This value is higher than the (wet) tensile strength of the glass frit (4.2 MPa), thus explaining the observed damage. As anticipated, the extent of damage was substantially less than what was observed when dehydration was allowed to proceed to completion, and recrystallization of mirabilite was allowed upon dissolution

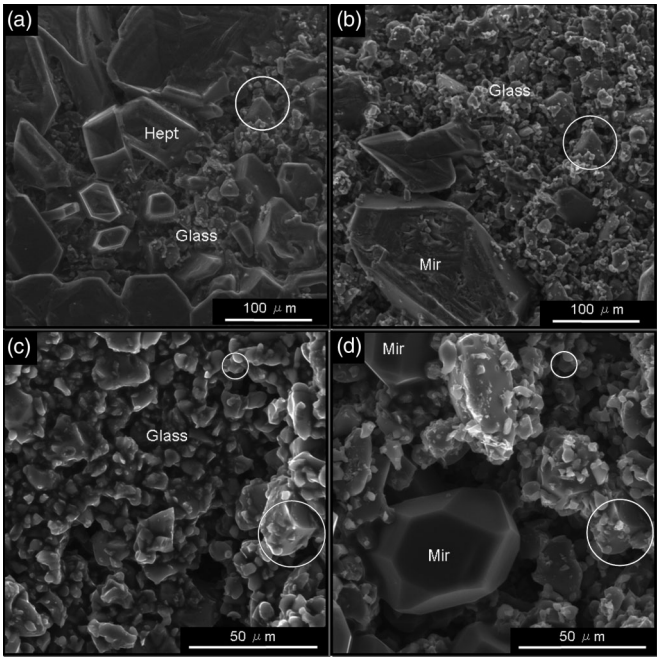

FIG. 4. ESEM images of sodium sulfate crystallization in porous glass. (a) Hydrated sodium sulfate crystals formed within and on the porous glass following drying at $RH > 64\%$ (no dehydration of hydrated phases was allowed to occur). The large prism-shaped crystals show a morphology consistent with heptahydrate (Hept) [12]. (b) Mirabilite (Mir) crystals formed after deliquescence and reprecipitation of hydrated crystals shown in (a). Loss of substrate grains is observed, which can only be attributed to the heptahydrate-mirabilite phase transition. (c) Surface features of the porous glass after the first crystallization event in which all of the crystals are beneath the surface and undetectable in ESEM. (d) Mirabilite crystals, identified by their equilibrium morphology, formed upon dissolution of thenardite and recrystallization. Changes in the surface topography of the porous glass substrate reflect significant damage associated with this second crystallization event (i.e., thenardite-mirabilite phase transition). White circles mark unchanged reference points on the substrate.

of the anhydrous phase [Figs. 4(c) and 4(d)]. Upon dissolution of thenardite at 2 °C, a solution forms with $\beta = 23.48$ with respect to mirabilite. Subsequent mirabilite crystallization leads to a Δp of 32.8 MPa, and P values that range between 3.21 MPa ($\phi_e = 0.11$) and 8.16 MPa ($\phi_e = 0.28$) according to the two scenarios described above. The last value is enough to significantly damage the porous glass, as observed here, and most building materials [21]. This evidence supports the theory that the thenardite to mirabilite phase transition is responsible for a great amount of the overall Na_2SO_4-induced physical damage to porous materials [7,21]. However, our results show for the first time that the coupled dissolution-precipitation of heptahydrate-mirabilite can also account for significant damage to the porous substrate, thus explaining experimental and field observations (Fig. 1) that show substantial damage by sodium sulfate crystallization during continuous evaporation [10,22].

Dissolution-precipitation mediated transitions between salt phases with contrasting solubilities (e.g., heptahydrate-mirabilite and thenardite-mirabilite) appear to be a general mechanism responsible for the buildup in supersaturation, explaining why salt systems with multiple phases (hydrated or anhydrous, metastable or stable) such as sodium sulfate, but also magnesium sulfate and sodium carbonate, are generally the most deleterious [9,22]. Damage associated with such phase transitions would only occur when the rate of dissolution of the precursor phase is higher than the crystallization rate of the stable one [24] and when there is a significant solubility (and surface energy) difference between precursor and stable phases. This gained knowledge helps in developing novel strategies to prevent salt damage to porous materials (i.e., use of crystallization promoters). Our results may also have important implications in other natural and industrial systems where crystallization and solvent-mediated phase transitions occur in a confined geometry.

This work has been supported by EC VII FP, Marie Curie Actions, Grant No. PITN-GA-2008-215360 and by the Spanish Government under Grant No. MAT2009-11332. One of us (E. R. A.) also acknowledges the Spanish Ministry of Science and Education for a Ramón y Cajal Grant. Additional funding was provided by the project P11-RNM-7550 and the research group RNM-179 (Junta de Andalucía, Spain). We thank the personnel of the CIC, University of Granada, for their help during TG, DSC, 2D-XRD, and ESEM analyses. We also thank Dr. R. Espinosa-Marzal for her help with nucleation density calculations and three anonymous referees for their comments and suggestions.

*Corresponding author:
carlosrn@ugr.es

[1] E. Ruiz-Agudo, C. Rodriguez-Navarro, and E. Sebastián-Pardo, Cryst. Growth Des. **6**, 1575 (2006).
[2] A. E. S. V. Driesschen, L. G. Benning, J. D. Rodriguez-Blanco, M. Ossorio, P. Bots, and J. M. Garcia-Ruiz, Science **336**, 69 (2012).
[3] E. H. Oelkers, S. R. Gislason, and J. Matter, Elements **4**, 333 (2008).
[4] G. W. Scherer, Cem. Concr. Res. **34**, 1613 (2004).
[5] H. K. Henisch, *Crystal Growth in Gels* (Pennsylvania State University Press, Pennsylvania, 1976).
[6] F. C. Meldrum and H. Cölfen, Chem. Rev. **108**, 4332 (2008).
[7] G. W. Scherer, Cem. Concr. Res. **29**, 1347 (1999).
[8] C. Rodriguez-Navarro, E. Doehne, and E. Sebastian, Langmuir **16**, 947 (2000).
[9] I. S. Evans, Rev. Geomorphol. Dyn. **19**, 155 (1970); A. Goudie and H. Viles, *Salt Weathering Hazards* (Wiley, Chichester, England, 1997).
[10] C. Rodriguez-Navarro and E. Doehne, Earth Surf. Processes Landforms **24**, 191 (1999).
[11] L. A. Rijniers, H. P. Huinink, L. Pel, and K. Kopinga, Phys. Rev. Lett. **94**, 075503 (2005).
[12] A. Hamilton, C. Hall, and L. Pel, J. Phys. D **41**, 212002 (2008).
[13] R. M. Espinosa-Marzal and G. W. Scherer, Acc. Chem. Res. **43**, 897 (2010).
[14] C. Rodriguez-Navarro, E. Doehne, and E. Sebastian, Cem. Concr. Res. **30**, 1527 (2000).
[15] E. Doehne and C. Price, *Stone Conservation: An Overview of Current Research* (The Getty Conservation Institute, Los Angeles, 2010).
[16] J. Thomson, *On the Disintegration of Stones Exposed in Buildings and Otherwise to Atmospheric Influence* (Report of the Annual Meeting, British Association for the Advancement of Science, London, 1862), p. 35.
[17] C. W. Correns, Discuss. Faraday Soc. **5**, 267 (1949).
[18] M. Steiger and S. Asmussen, Geochim. Cosmochim. Acta **72**, 4291 (2008).
[19] R. M. Espinosa-Marzal, A. Hamilton, M. McNall, K. Whitaker, and G. W. Scherer, J. Mater. Res. **26**, 1472 (2011).
[20] R. M. Espinosa-Marzal and G. W. Scherer, Environ. Geol. **56**, 605 (2008).
[21] R. J. Flatt, J. Cryst. Growth **242**, 435 (2002).
[22] E. Ruiz-Agudo, F. Mees, P. Jacobs, and C. Rodriguez-Navarro, Environ. Geol. **52**, 269 (2007).
[23] See Materials and Methods in Supplemental Material at http://link.aps.org/supplemental/10.1103/PhysRevLett.109.265503 for details of salt crystallization tests, and calculation of drying kinetics, effective crystallization pressure, and nucleation density.
[24] P. T. Cardew and R. J. Davey, Proc. R. Soc. A **398**, 415 (1985).
[25] A. Putnis, Rev. Mineral. Geochem. **70**, 87 (2009).
[26] G. W. Scherer, J. Am. Ceram. Soc. **73**, 3 (1990).
[27] D. Benavente, M. A. Garcıa del Cura, and S. Ordóñez, Construct. Build. Mater. **17**, 113 (2003).
[28] S. Veran-Tissoires, M. Marcoux, and M. Prat, Phys. Rev. Lett. **108**, 054502 (2012).
[29] M. Telkes, Ind. Eng. Chem. **44**, 1308 (1952).
[30] K. Linnov, A. Zeunert, and M. Steiger, Anal. Chem. **78**, 4683 (2006).
[31] A. Hamilton and C. Hall, J. Anal. At. Spectrom. **23**, 840 (2008).
[32] *International Critical Tables (ICR) National Research Council*, Vol. III (McGraw-Hill, New York, 1928).